SAE INTERNATIONAL

Experimental Investigations of Vehicle Base Drag Reduction Using Passive Jet Boat-Tail Flow Control

2014-01-2448
Published 09/30/2014

William Bradford Bartow, Andres C. Moreyra, Trevor Hirst, Gregory H. Woyczynski, Alexis Lefebvre, and Gecheng Zha
University of Miami

CITATION: Bartow, W., Moreyra, A., Hirst, T., Woyczynski, G. et al., "Experimental Investigations of Vehicle Base Drag Reduction Using Passive Jet Boat-Tail Flow Control," SAE Technical Paper 2014-01-2448, 2014, doi:10.4271/2014-01-2448.

Abstract

This study is focused on the detailed experimental investigation of jet boat-tail (JBT) passive flow control bluff body models to reduce the base pressure drag. The JBT technique is employed through an open inlet at the leading edge of the bluff body along with a circumferential jet at the trailing edge in order to energize the base flow using the high kinetic energy flow from freestream. As a consequence, entrainment of the main flow into base flow region is initiated earlier downstream. A reduction in the turbulent fluctuation of the wake can be observed in addition to a decrease of the recirculation region velocity. Using 2D/3C Particle Image Velocimetry (PIV), two models with different inlet sizes are tested. The large flow rate model is designed with an inlet area 4.7 times greater than the other JBT prototype. The wind tunnel experimental results show a substantial reduction in the wake width and depth for the two models, which indicates a significant drag reduction. Moreover, mean velocity vector plots from PIV measurements at the mid-plane location suggest their flow fields differ significantly due to the nature of the passive jets employed. The Jet1 model initiates the large coherent structures and flow entrainment earlier than the baseline model even though the jet momentum is small. The Jet2 generates paired vortices in the shear layer due to the high jet momentum and entrain main flow to the base region. The experimentation is performed at a Reynolds number of $Re = 2.55\times10^5$. In order to investigate the effects at higher Reynolds numbers, Computational Fluid Dynamics (CFD) is used to model the flows using Large Eddy Simulation, which shows that the drag reduction is more effective at high Reynolds number.

Introduction

Aerodynamics of commercial road vehicles continues to play a crucial role in vehicle design and are currently the focus of many ongoing research topics. In general, we can consider road vehicles, in particular commercial heavy duty trucks, to be bluff bodies close to the ground [1]. For aerodynamicists, reducing the base pressure drag in order to optimize bluff bodies is usually the main focus of design enhancements. According to a study produced by Drollinger, base pressure drag for commercial tractor trailers contributes to 20% of total vehicle drag while the stagnation pressure component can contribute up to 40% [2]. These numbers reveal not only the significant contributions to drag associated from the pressure forces but also the significant gains that can be made from enhancements to eliminate their effects. Today's efforts to continuously increase aerodynamic efficiency drives us towards new and innovative designs that not only ensure a more environment friendly commercial vehicles but also an increasing role in aerodynamics in vehicle design for the foreseeable future.

Major base drag reduction methods used today include splitter plates, splitter wedges, base bleed, boat tailing and various types of serrated trailing edges [3,4,5]. Tanner gave an excellent overview of these passive flow control methods in which it is noted they do not consume energy while reducing drag [6]. Although these methods do not consume energy, there are limitations to each application. The splitter plates are lengthy and are difficult to apply due to the space and stability limitations. Boat tailing [7] is often used for tractor-trailer drag reductions but increases the overall length of the vehicle which is impractical per traffic regulations and prohibitory for loading purposes [8]. The base bleed concept [9,10] requires opening a hole in the center of the base of a bluff body to allow a vortex in a counter rotating direction to break the focused vortices and in so doing increase the base pressure while reducing drag. However, there are few industrial applications that permit opening holes at the center of the base.

Given the limitation of the current base drag reduction methods, a new passive flow control method is developed to reduce the base drag without creating blockage in the base area as seen in traditional boat tailing techniques [11,12,13,14]. Proof of concept for the new method is provided via wind tunnel testing and preliminary Large Eddy Simulation (LES) results [14]. This article expounds on that research by providing detailed experimental results as found by utilizing Particle Image Velocimetry (PIV) and analysis of same.

Jet Boat Tail Concept

To demonstrate the advantage of passive flow control incorporated into a commercial vehicle application, a bluff body with a sharp trailing edge surface is used as the a baseline model for comparison. Modifications to the baseline model are utilized to simulate the enhanced commercial vehicle geometry observed in the wind tunnel experimentation. PIV is used to measure the effects of the passive flow control on the recirculation region and the corresponding downstream wake.

The base region of the bluff body model is considered to be analogous to the base region of a commercial vehicle due to the similarities derived from the nature of the unsteady bluff body separated flow that both exhibited at the trailing edge of each respective geometries. Despite their similarities, significant differences in the fluid dynamic properties exist such as the boundary layer thickness at the trailing edge of the commercial vehicle trailer do exist and may have a positive influence on the behavior of the free shear layer that develops with the passive jet models. A larger presence of turbulence in the thicker boundary layer before separation at the trailing edge of the model could enhance the results of the passive jet mixing and increase the wake area reductions measured, thus making the application to commercial vehicles more promising. In order to facilitate the application of the passive jet in the base region of a trailer, free stream fluid will be ducted from the boundary layer over the trailer surface and injected into the low pressure base region through a similar configuration that is employed for the bluff body prototypes.

The baseline model cross sectional sketch is illustrated in Figure 1, which is observed to create a large wake behind the bluff body model in addition to flow separation at the trailing edges. Figure 2 is a cross section sketch of the bluff body model in which the configuration of a passive flow control is incorporated into the model geometry. The flow control concept is to utilize an open inlet at the front leading edge of the configuration, introduce airflow via a converging duct, and eject the flow through a circumferential jet from the model base surface at an angle toward the center line of the wake region.

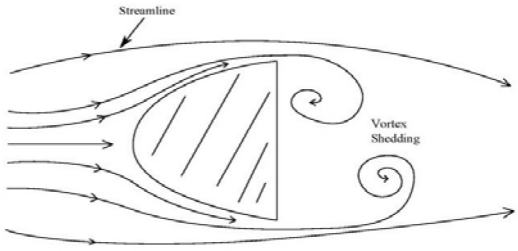

Figure 1. Vortex shedding flow structure of a bluff body model with a sharp trailing edge.

Figure 3 illustrates the expected reduced wake region. The effect is equivalent to adding a boat-tail to the model geometry, hence named as Jet Boat Tail (JBT).

This flow behavior is representative of potential drag reduction for square back commercial vehicle geometries due to the incorporation of a high kinetic energy passive jet in the base recirculation region. The jet harnesses the energy from the free stream by unsteady jet mixing with the main flow via large vortex structures, entrains the main flow to energize the base flow which reduces the wake size and over all turbulence fluctuation, as illustrated in Figure 3. The advantage of the passive flow control application is it requires no additional energy input.

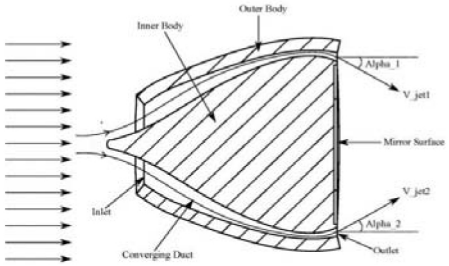

Figure 2. Cross sectional drawing showing internal geometry of a jet boat tail model.

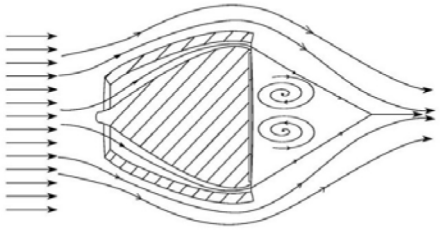

Figure 3. Expected flow structure with the jet boat tail effect influence.

JBT Models

In this study, three bluff body models are tested and measured using Stereoscopic Particle Image Velocimetry (PIV). A baseline model is used to compare the changes with two passive flow control models that employed the JBT as shown in Fig. 4. The overall length of the baseline model is 129.30mm. Its semi-major axis measured 190.5mm and has a semi-minor axis length measured 126.18mm. In this configuration, an inlet cap is used and secured to the leading edge of the model in order to simulate a baseline configuration. In order to create the Jet1 passive flow control model, the end cap is removed from the baseline model as shown in Figure 5. Preliminary testing results for the baseline and Jet1 model are

presented in [14]. A third model is included for this study. The new model measured the effects of a large inlet area and higher velocity jet on the wake recirculation region as shown in Figure 6. The estimated blockage for the models tested is calculated to be 7% of the wind tunnel test section area.

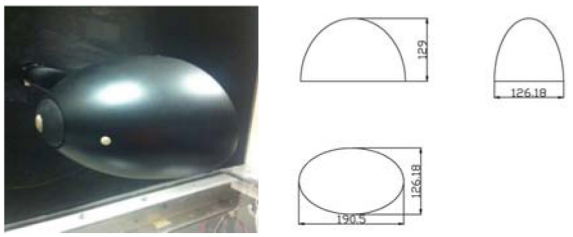

Figure 4. Baseline Model and Dimensions

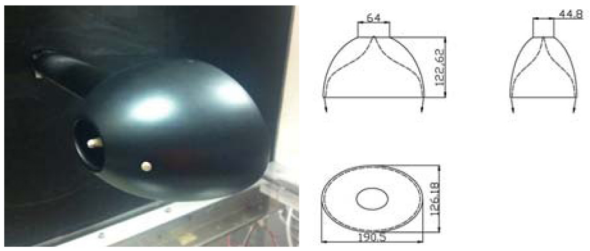

Figure 5. Jet1 Model and Dimensions

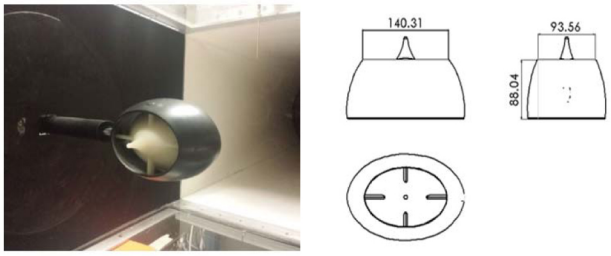

Figure 6. Jet2 Model and Dimensions.

Particle Image Velocimetry

All results were obtained at the University of Miami Wind Tunnel Research facility in an Open-Circuit Wind Tunnel. The tunnel test section dimensions are 24×24×48 (61.0cm × 61.0cm×121.0cm) [15,16]. The wind tunnel test section walls are comprised of 0.75 (1.90cm) acrylic on all four sides in order to provide optimum optical analysis from multiple perspectives. The results presented in the PIV experimentation are from wind tunnel tests at V_{Total} = 10.0 m/s (Re = 8.52×10^4) and V_{Total} = 30.0 m/s (Re = 2.55×10^5) using a reference length (L) of L= 129.30mm in order to calculate the Reynolds number. All three configurations are mounted to an Aluminum strut that is attached to the load cell sting, extending the models into the center of the test section. An Advanced Mechanical Technology, Inc.(AMTI) MC2.5B-2K-SS-5024, 6 channel load cell is used to measure preliminary drag force measurements by subtracting the drag contribution of only the aluminum strut from the total drag force measurements recorded with each model tested. The maximum range of the load cell in the Fx and Fy directions are 1000 lb (4448N) and 2000 lb (8896N) in the Fz directions [16] which prevented accurate measurements with the resolution necessary for the range observed from the bluff body models.

A Lavision Digital Particle Velocimetry (DPIV) system is utilized to perform the PIV experimentation in this study. The digital PIV system includes a Litron 135mJ Double Pulse Nd:YAG Laser and two Lavision proX2M series CCD Camera capable of a maximum recording rate of 14Hz in a stereo PIV configuration. Results presented here are from studies conducted acquiring 400 samples per experiment at approximately 6Hz [17]. An uncertainty analysis performed according to guidelines provided by the International Towing Tank Conference resulted in a maximum uncertainty of 3.75% [18]. PIV velocity calibration measurements recorded are within 1% of measured wind tunnel test section free stream velocity. Force measurements are not recorded in this study due to the sensitivity of the available load cell in the wind tunnel facility. Additionally, influence in the drag reduction to the stagnation region due to the passive jet inlet is not analyzed as well. Applied to a square back tractor trailer, the ingestion of the free steam flow would be originating from the free stream around the trailer rather than from the stagnation region by the radiator of the commercial vehicle. The aim of this study is to analyze the influence of the passive jet on the recirculation region behind a bluff body model.

Table 1. PIV Instrumentation and Data Processing.

Target Flow of Measurement	
Target Flow of Measurement	2D/3C Air Flow in Wind Tunnel Section
Uniform flow speed (m/s)	30
Tracer Particle	Di-Ethel Hexel Sebecate
Average Diameter dp(mm)	0.001
Light Source	Duble Pusle Nd:YAG Laser
Laser Power	800 mJ
Laser Sheet Thickness	1.0mm
Time interval dt (μs)	38
Image Detection	
Camera	
Spatial Resolution	1600 x 1200 pixels
Sample Rate	~6 Hz
Pixel Size	.0074 mm x .0074 mm
Data Processing	
Pixel Unit Analysis	Stereo Cross Correlation Method
Correlation Area Size	64 x 64 pixels
Serach Area Size	32 x 32 pixels
Interegation Window Overlap	50% Firstpass, 75% Seccond Pass.

Results

V=30m/s, Re=2.55×10^5

Based on the following basic aerodynamics drag equation

$$D = \int_{\delta} \rho u(u_\infty - u)dy \quad (1)$$

where δ is the width of the wake, a reduction in the overall area of the wake and the velocity deficit depth will cause a reduction in the drag [19]. Contained in this section are the results from experimental measurements at V_{Total} = 30m/s, Reynolds number of Re = 2.55×10^5, demonstrating the JBT passive flow control models substantially reducing the wake width and velocity deficit thus decreasing the overall drag. All PIV measurements presented are collected on the mid-plane of each configuration as illustrated in Figure 7. The z axis value of z = 0 is used for location of the plane in which the centerline mean total planar velocity measurements are recorded. The velocity contour plots shown in Figures 8, Figures 9, Figures

10 are the planar velocity contours of the baseline and two passive flow control configurations. The results obtained are time averaged from 400 samples collected at a sample rate of 6Hz.

Observed in Figures 8, Figures 9, Figures 10 are the mean total planar velocity V_{Total} measurements parallel to the free stream flow in which both the Jet1 and the Jet2 configurations display a substantial reduction in the wake area documented by the mean velocity streamlines

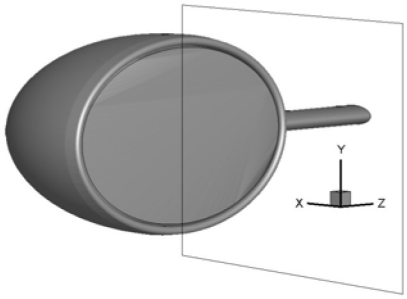

Figure 7. PIV planar view showing coordinate axis and orientation.

. The Jet2 model, which has a 4.7 times larger inlet area and hence significantly more jet mass flow and momentum, displays a slightly larger wake area reduction than the Jet 1 configuration documented by the mean velocity streamlines in Figure 10.

The mean velocity profiles recorded at 1.5 model lengths downstream are presented in Figure 11. The influence of the passive flow control on the wake behind the bluff body can also be observed in the reduction of the velocity profile magnitude at the 1.5 model lengths downstream for both Jet1 and Jet2 models. Despite the larger inlet to outlet ratio of the Jet2 design, the measured difference between the two flow control configurations is mainly in the recorded velocity magnitude at the centerline of the wake profile. The results displayed in Figure 11 also indicate the velocity profiles for both Jet1 and Jet2 models have a similar velocity profile at 1.5 model lengths downstream. This suggests that a smaller jet inlet can obtain similar downstream wake velocity profiles of a larger inlet. Additionally, both passive jet models display a reduction in the recirculation region velocity measured as well.

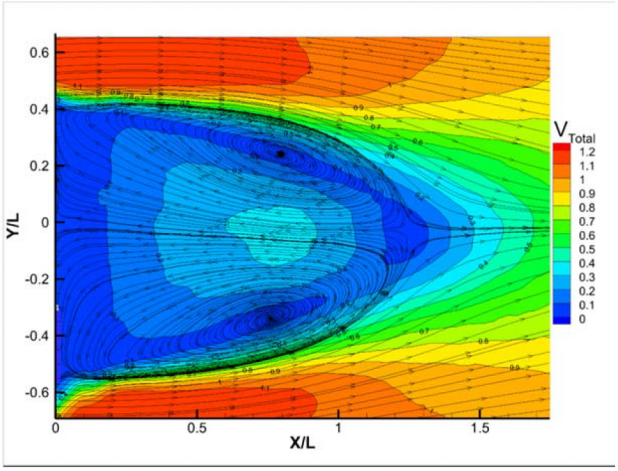

Figure 8. Baseline average velocity contours and streamlines at V_{Total} = 30.0 m/s Re = 2.55×10^5

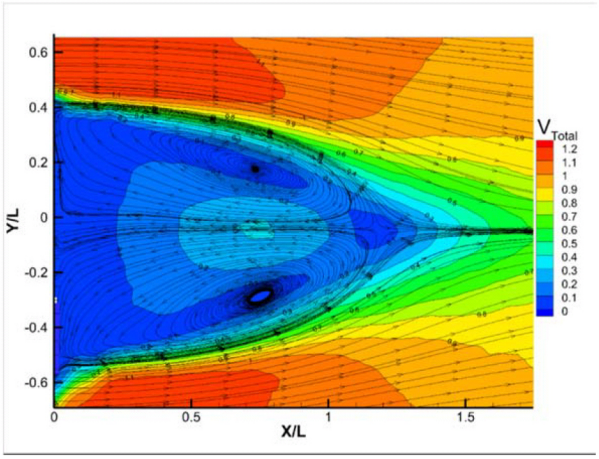

Figure 9. Jet1 average velocity contours and streamlines at V_{Total} = 30.0 m/s Re = 2.55×10^5

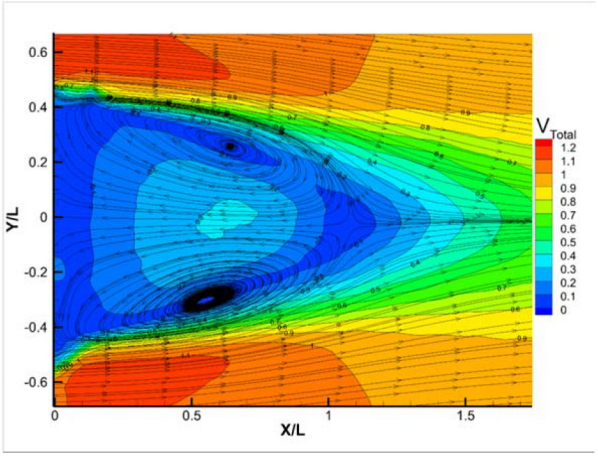

Figure 10. Jet2 average velocity contours and streamlines at V_{Total} = 30.0 m/s Re = 2.55×10^5

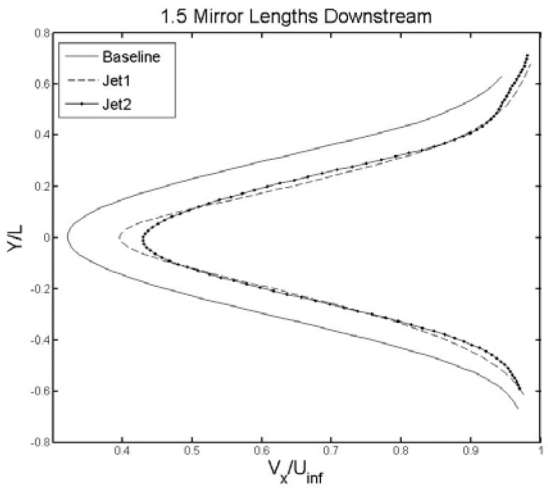

Figure 11. Average velocity profile at 1.5 model lengths downstream for V_{Total} = 30.0 m/s Re = 2.55×10^5

The coherent structures that develop in the shear layer behind the bluff body are the result of the high energy free stream flow interacting with the recirculation region behind the model. The free shear layer influenced by the passive jet impinging is observed through alteration of the coherent structures created in the recirculation region. It is reported by Wu et. al. that two process occurring that allow for the transfer of energy from the free stream shear layer to the low energy wake region, one of which is the cascading transition of energy transfer from large scale vortices to small scale vortices [20]. Although this process occurs naturally in the baseline wake region, the jet interaction with the existing wake structure enhances the properties of the region and resulted in reduced mean velocity streamline profiles and velocity profiles at downstream locations.

As observed from Figure 12, Figure 13, Figure 14, implementing the passive jet flow control and the effects of the jet mixing on the shear layer are quite evident in the difference of the vortex shedding that occurs behind the bluff body model. Figure 12 shows the coherent shedding nature of the shear layer generated by the free stream and the recirculation region that is noticed downstream of the baseline bluff body model. It is observed that the coherent vortical structures downstream in the wake shear layer are altered by both passive flow control models. The Jet1 model is observed to create passive jet oriented upward towards the free stream shear layer whereas the Jet2 configuration produced a jet oriented streamwise due to the higher momentum. The Jet1 coherent production can be observed in Figure 13. The coherent structures produced by the Jet1 model are closer to the trailing edge of the base region and possess different characteristics as well. It is observed that the coherent structures display what is regarded as a forced coherent structure described by Wu et. al. [20].

The coherent structures produced by the Jet2 configuration are displayed in Figure 14. The modified coherent production for the Jet2 model is also recognized to be closer to the trailing edge of the base region as well. In addition, the coherent structures produced are observed in the shear layer between the Jet2 interface and the recirculation region as well as the Jet2 interface and the low velocity region between the free stream shear layer and the passive jet. This behavior is also supported by the velocity profile at 5% model lengths downstream from the base of the model in Figure 21 in the preceding sections.

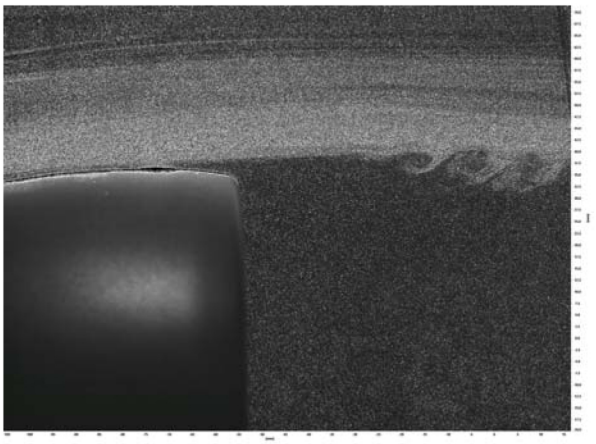

Figure 12. Baseline instantaneous coherent vortex shedding at V_{Total} = 10.0 m/s Re = 8.52×10^4

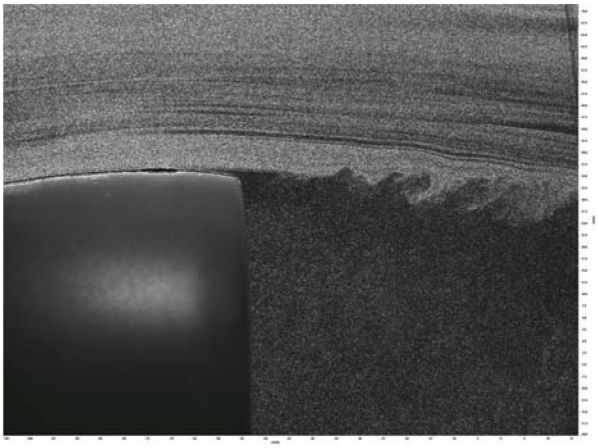

Figure 13. Jet1 instantaneous coherent vortex shedding at V_{Total} = 10.0 m/s Re = 8.52×10^4

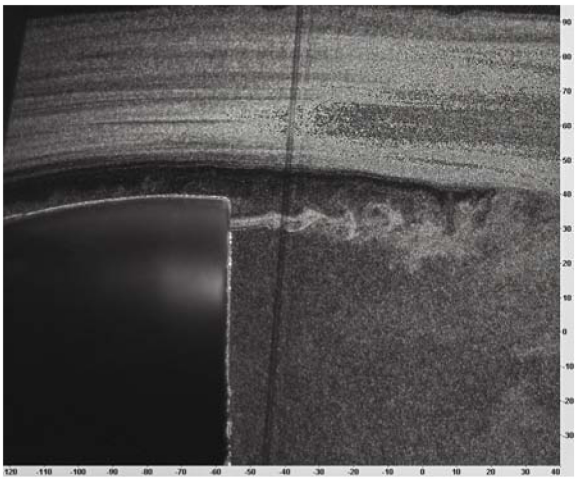

Figure 14. Jet2 instantaneous coherent vortex shedding at V_{Total} = 10.0 m/s Re = 8.52×10^4

These new vortical structures can be described as the coherent vortex nature of paired vortices [20] and are a direct result of the jet impinging on the high energy free stream flow. Evident in Figure 13 is the intersection of the jet flow with the main flow shear layer. This PIV image displays a distinct region where the free steam shear layer intersects with the Jet1 passive jet. The behavior of the two passive jets in the trailing edge region supports the notion that the jet mixing is unique to the two passive flow control models tested and their configurations generate unique flow behaviors in the recirculation regions due to their influence.

Instantaneous PIV images taken of the full wake area for the Jet1 and Jet2 models display the different behavior of each passive jet model on the immediate trailing edge region for the full wake view in Fig. 15, which are processed to eliminate the background low intensity light to accentuate the flow seeding more clearly.

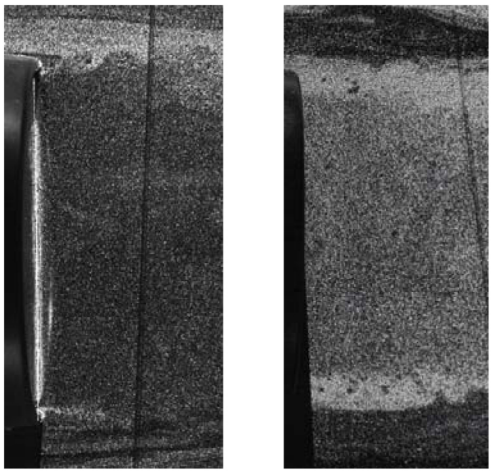

Figure 15. Jet1 (Left) and Jet2 (Right) Instantaneous PIV with vortices for V_{Total} = 30.0 m/s Re = 2.55×10^5.

Investigation of the flow in the immediate wake region behind the bluff body model indicates that the high velocity passive flow control jet of the Jet2 model created small scale vortices in the shear layer downstream of the trailing edge. These are observed through the darker circular regions suggesting the absence of seeding particles in the recirculation region of the wake. Theses vortices are observed to be the product of enhanced vorticity in the shear layer developed behind the Jet2 model due to the orientation of the passive jet parallel with the free stream flow.

Figure 16 and Figure 17 display the instantaneous velocity vectors of the passive flow control jet for both Jet1 and the Jet2 configurations. The behavior of the Jet2 model is observed to possess a higher flow velocity and momentum as it is recorded further downstream than the Jet1 model. The Jet2 mixes with the free stream shear layer as the wake converges towards the center of the recirculation region. This deviates from the recorded behavior of the Jet1 configuration in which the jet is observed to mix with the shear layer immediately following the trailing edge as it is oriented outward, towards the free stream flow. The orientation of the Jet2 passive jet is more clearly documented by the PIV mean velocity vector plots of the three models that are tested in Figure 18, Figure 19, Figure 20.

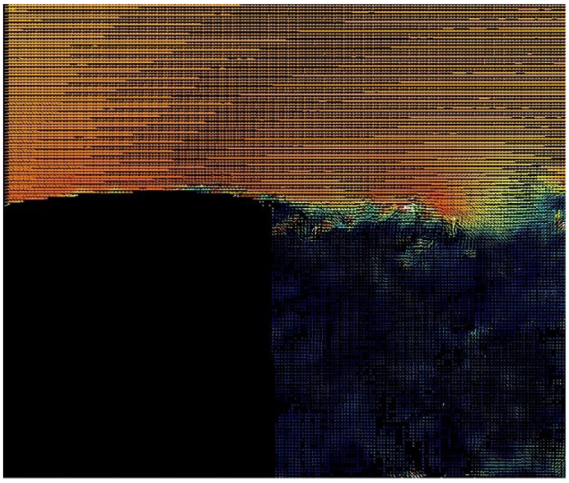

Figure 16. Jet1 instantaneous velocity vectors at V_{Total} = 30.0 m/s Re = 2.55×10^5.

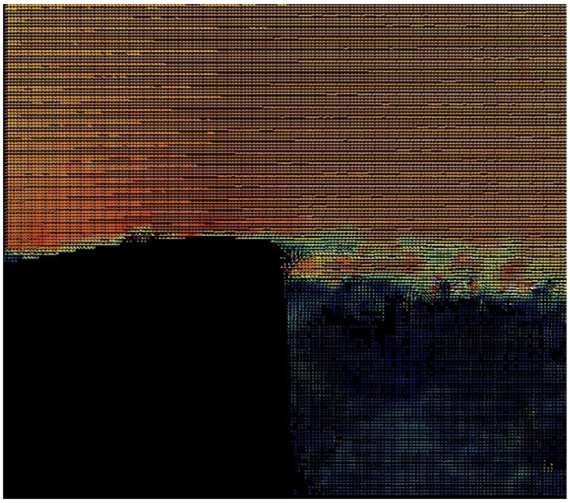

Figure 17. Jet2 instantaneous velocity vectors at V_{Total} = 30.0 m/s Re = 2.55×10^5.

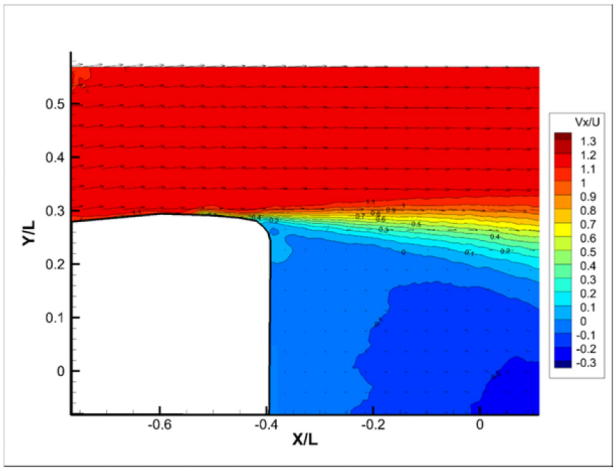

Figure 18. Baseline Vx mean velocity contour at V_{Total} = 30.0 m/s Re = 2.55×10^5.

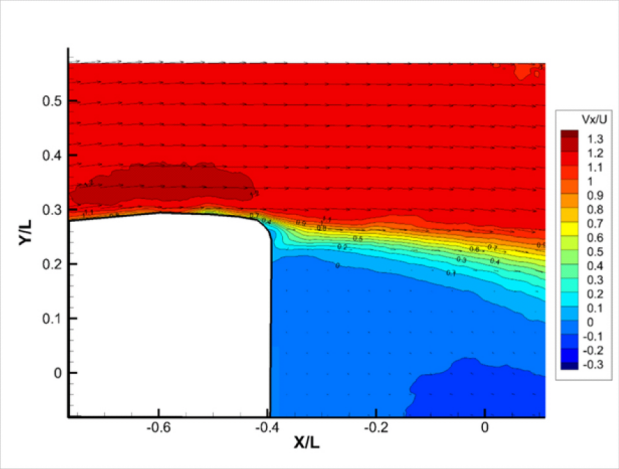

Figure 19. Jet1 Vx mean velocity contour at V_{Total} = 30.0 m/s Re = 2.55×10^5.

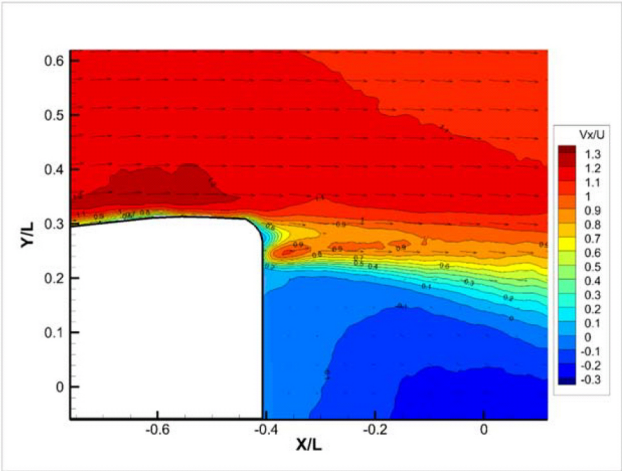

Figure 20. Jet2 Vx mean velocity contour at V_{Total} = 30.0 m/s Re = 2.55×10^5.

Figure 18, 19, 20 are the mean velocity contours for all three JBT models. The results displayed in each figure are normalized by the free stream wind tunnel velocities recorded during each independent experiment. The baseline model shown in Figure 18 displays the expected flow separation of the free shear layer from the trailing edge of the baseline bluff body model.

The mean velocity profile displayed in Figure 19 is the recorded Jet1 configuration behavior and documents the influence of the passive jet in reducing the recirculation region height depicted by the velocity contours observed. Velocity contours observed for the Jet1 model show an Increase of high momentum flow in the wake region. The reduced recirculation region height is also observed from the initiation of the free shear layer at a value closer to the centerline of the recirculation region. In addition to the influence of the passive jet on the formation of the shear layer, the flow around the body surface is also observed to be affected from the passive jet as a well. This can be observed in the region of accelerated free stream velocities as the flow approaches the trailing edge of the model. This acceleration is not observed in the baseline model and is directly attributed to the introduction of the passive jet.

The influence of the Jet2 configuration in the base region is also documented to have a reduction in the recirculation height similar to that of the Jet1 model. The reduction in recirculation region behind the trailing edge for the model can be observed in Figure 20 by the increased presence of high momentum flow in the shear layer region of the wake. The increased jet flow velocity is noticeably more pronounced for the Jet2 configuration as is the reduction of the wake area height. Also noticeable is the location of which the higher energy jet for the Jet2 model intersects with the free stream shear layer as it can be observed to be further downstream than the location observed in the Jet1 model. It's believed this is the cause of the similar wake profile between Jet1 and Jet2 despite their unique passive jets configurations. As the high velocity flow from the base intersects with the free stream shear layer of similar flow velocity, the mixing of the two streams causes the convergence process to be delayed further down stream. This is also evident in the comparison of the mean velocity profiles in Figure 9 and in Figure 10. The Jet1 model shown in Figure 9 displays a sharp convergence of the wake profile whereas the Jet2 profile in Figure 10 shows a more gradual progression downstream. Figure 21 shows the profile for the Vx component of V_{Total} at the distance of 5% of the model length from the base of the model. A comparison of all three models are shown in addition to the immediate corresponding reductions in the wake profile height attributed to the passive flow control jets.

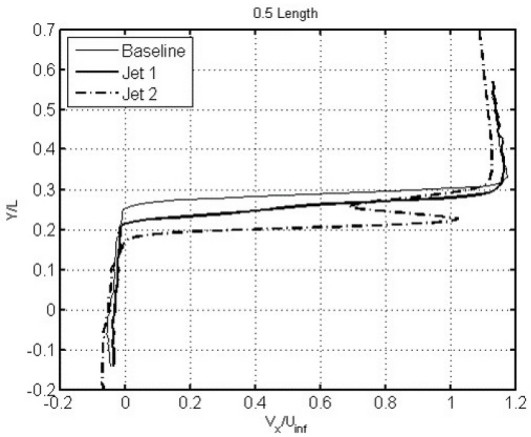

Figure 21. V_X mean velocity profile at 5 of the model length down stream. V_{Total} = 30m/s Re = 2.55×10^5.

The Jet1 configuration displayed a gradual slope of the velocity gradient in the shear layer which is contrasted by the behavior of the Jet2 model. The gradient profile of the Jet2 model is observed to display multiple regions of shear layers as is seen in Figure 14 and is also documented by the reverse in the recorded velocity magnitude before continuing to converge with the free stream. Moreover, despite the lower mass flow rate of the Jet1 passive jet, the velocity profiles are noticed to possess the similar gradient profiles following the change in magnitude of the Jet2 passive jet. The flow characteristic of the Vz component for the wake area also displays interesting flow behavior as well. The mean Vz component of velocity for the

jet1 recirculation region displays a pocket of high magnitude, positive Z component of flow as can be seen in Figure 22. It is suggested by this documented behavior that the introduction of a passive flow control jet could produce sustained circumferential velocity components where the jet mixes with the shear layer.

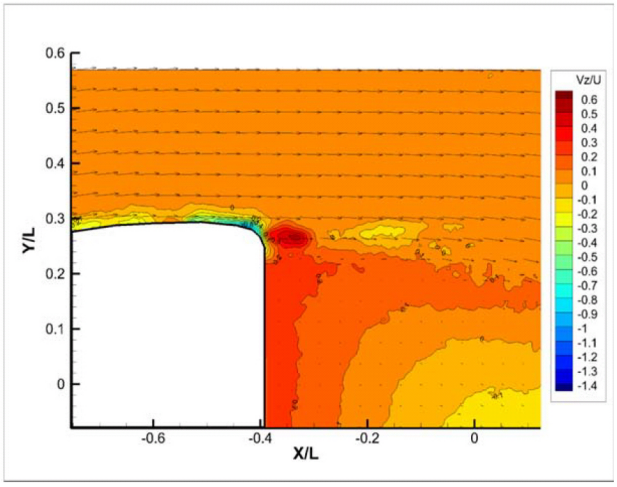

Figure 22. Jet1 Vz Velocity contour at V_{Total} = 30.0 m/s Re = 2.55×10^5.

Large Eddy Simulation Results

Computational Fluid Dynamic simulations are used to model the bluff body behavior at higher Reynolds flow due to the limitations of the wind tunnel and its maximum Reynolds number of Re = 4×10^5. In order to computationally investigate the flow structure of the bluff body model, Large Eddy Simulation (LES) is used to evaluate the models at Reynolds number of 2.7×10^6 corresponding to a full scale tractor trailer width at highway speeds. Implicit LES methodology used by Shen and Zha in [21] is adopted in the CFD analysis utilizing Roe Scheme with the 3rd Order Weighted Essentially Non-Oscillatory (WENO) Scheme for the inviscid fluxes. Roe scheme is a Riemann solver to resolve flux at a control volume interface, often used to capture both smooth flow and discontinuities such as shock waves [21]. The 3rd order WENO scheme is a reconstruction procedure to achieve a 3rd order scheme for the Roe Scheme flux calculation [22,23]. Second order differencing is used for the viscous terms. The normalized nondimensional physical time step(t V_{Total} /L) of 0.02 is used.

Mesh

Structured meshes are used in all the three cases. To model the computation flow field, mesh sizes utilized to model the baseline bluff body is 6×10^6 for the baseline configuration. A mesh size of 3×10^6 is applied for Jet 1 and Jet 2 configurations. Figures 23 and Figure 24 display the mesh topology of the mid-cross section of the baseline model and Jet1 model. The far field boundary of the mesh is located at 20 times the length of the bluff body away from the model. A similar but separate mesh is also generated for the Jet2 configuration but is not shown here in this article. The mesh is in high quality with Y+ =1 on all the wall surface. The mesh refinement study gives similar results. The mesh topology for the jet model and the baseline model is not exactly the same since the geometry configurations are different. This is the reason that the Jet1 mesh size is smaller.

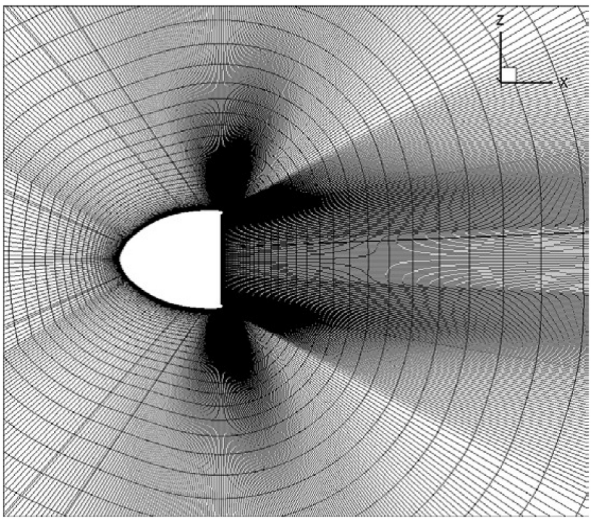

Figure 23. Cross-section view of the Baseline mesh for the bluff body model.

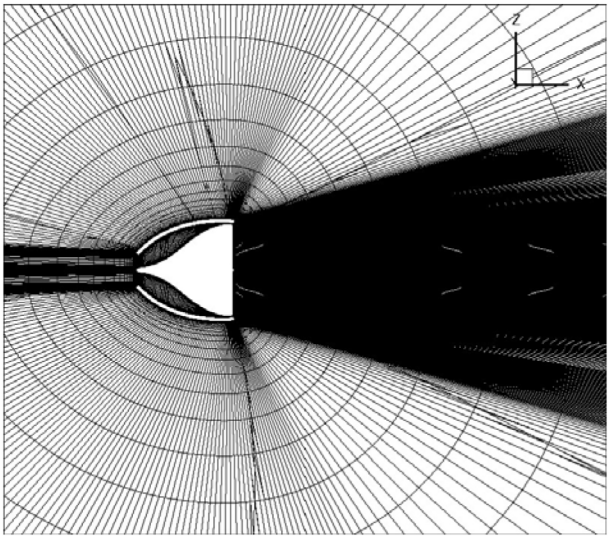

Figure 24. Cross-section view of the Jet1 mesh for the passive flow control model.

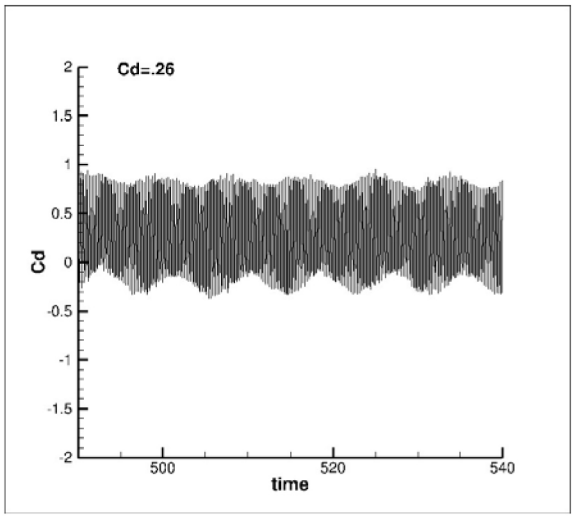

Figure 25. Recorded coefficient of drag measurement from CFD analysis for the Jet2 model.

Figure 25 shows the time history of the computed drag coefficient of the Jet2 design, which indicates the unsteady nature of the flow field in the fluctuations of the drag coefficient recordings. The Drag coefficients represent drag measurements for the complete bluff body model, which incorporated both the outer surface and inner geometry. An average drag coefficient of Cd=.26 is obtained for the Jet2 passive flow control model. Due to the range of the load cell in the experimental wind tunnel facility, the sensitivity is not high enough to use in a comparison between the computational results obtained.

Vortex shedding is an oscillating flow that occurs when fluid flows past a bluff body at certain speeds. In this type of flow, vortices are created at the rear base region. These vortices continuously detach from the trailing edge of the body creating a fluctuation in drag as seen in Figure 25 for the Jet2 model. Table 2 summarizes the drag coefficients of the different models at the experimental Reynolds number of 2.56×10^5. The data indicated that increasing the inlet size from the Jet1 to the Jet2 model greatly decreases the drag. The drag reduction is more significant for the high Reynolds number of road vehicles as indicated in Table 3.

Table 2. Coefficient of Drag for all three models calculated by CFD. V_{Total} = 30m/s $Re=2.56\times10^5$.

	Cd	Drag Reduction
Jet 2	0.26	40.91%
Jet 1	0.34	29.41%
Baseline	0.44	

Table 3. Coefficient of Drag for all three models calculated by CFD. $Re=2.6\times10^6$.

	Cd	Drag Reduction
Jet 2	0.22	64.52%
Jet 1	0.37	56.45%
Baseline	0.62	

Flow Field

Figure 26, Figure 27, Figure 28 display the instantaneous velocity contours normalized by the free stream at the semi-major axis plane section (y=0 section) for all three models. The wake width of Jet1 and Jet2 are significantly reduced when compared with the baseline model and correlates well with PIV data acquired experimentally. CFD results confirm the wake of the Jet2 model is the narrowest of the three due to the stronger jet momentum in the base region. In addition, the Jet2 model has higher jet velocity than the Jet1 model as a result of the greater captured mass flow rate due to a larger inlet area. This confirms the experimental data as demonstrated in the instantaneous velocity vector plot for the Jet2 configuration in Figure 17. Figure 26 displays wave like features extending into the free stream flow and are most likely numerical artifacts.

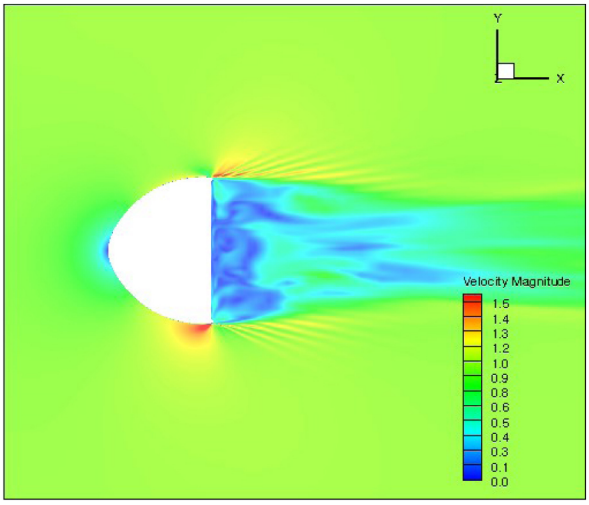

Figure 26. Instantaneous CFD Velocity contours for Baseline bluff body model. V_{Total} = 30m/s $Re=2.56\times10^5$.

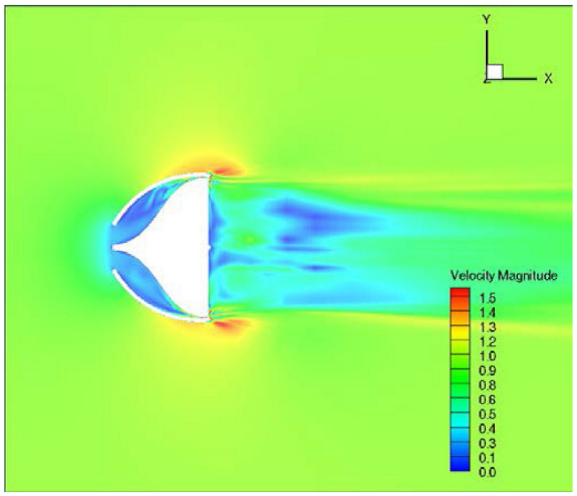

Figure 27. Instantaneous CFD Velocity contours for Jet1 bluff body model. V_{Total} = 30m/s Re=2.56×10^5.

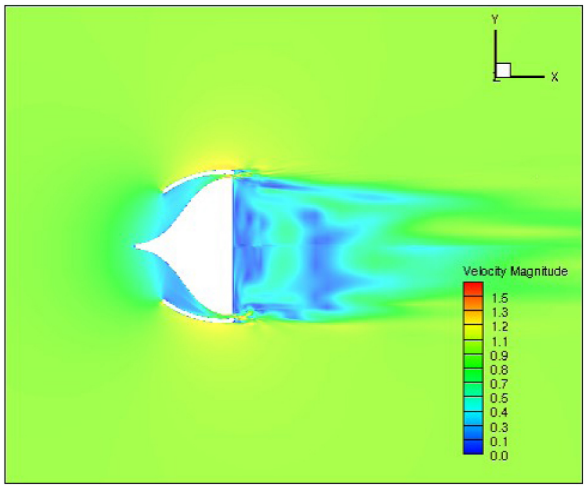

Figure 28. Instantaneous CFD Velocity contours for Jet2 bluff body model. V_{Total} = 30m/s Re=2.56×10^5.

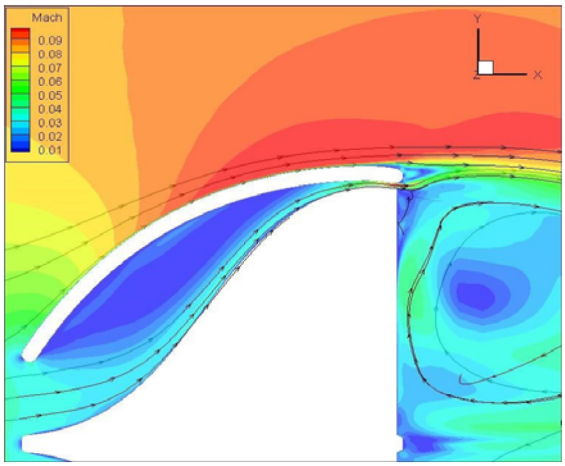

Figure 29. Instantaneous CFD Velocity contours for Jet1 bluff body model with high velocity passive jet. V_{Total} = 30m/s Re=2.56×10^5.

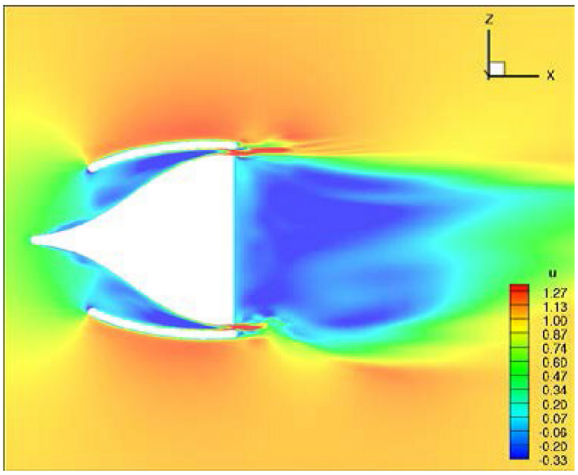

Figure 30. Instantaneous CFD Velocity contours for Jet2 bluff body model with high velocity passive jet pulsing. V_{Total} = 30m/s Re=2.56×10^5.

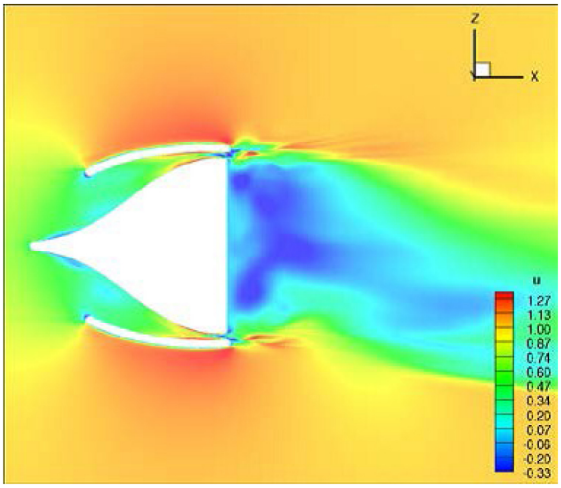

Figure 31. Instantaneous CFD Velocity contours for Jet2 bluff body model at same time step as Figure 31 but different cross sectional location with high velocity passive jet pulsing. V_{Total} = 30m/s Re=2.56×10^5.

The narrower recirculation region due to the high velocity, high momentum jet is demonstrated in Figure 28. Another observed phenomenon in the recirculation region is the behavior of the passive flow control jet. CFD data presented in Figure 29 and Figure 30 capture similar flow behaviors that are seen in the PIV experimentation. As can be observed in Figure 29 the passive jet of the Jet1 design reaches a maximum speed at the jet exit and is oriented outward towards the free stream as it exits the jet in the base region and agrees with the PIV data presented in Figure 16. CFD data confirmed this behavior is due to the higher static and total pressure of the jet.

The Jet2 behavior in Figure 30 also displays similar flow behavior as is recorded by PIV in Figure 17. Additionally, comparing the jet magnitude at different cross-sectional locations for the same time step reveals that the passive jet is pulsing and varying in magnitude with time. Mid plane slices taken at the same reference time from different location show that the jet velocity is indeed changing throughout the circumferential slot region. This CFD data is compiled into an

animation, which uncovers the behavior of pulsating nature in which the jet transitions from high velocity, high momentum flow velocity to low intensity/transformative states periodically. The pulsing of the jet is caused by the vortex shedding in the base region that creates pressure oscillation. The jet velocity is determined by the pressure. When the pressure oscillates to a high value, the jet velocity is low. Vice versa, when the pressure is low, the jet velocity is high.

Conclusions

The JBT passive flow control bluff body design is successful in reducing the overall aerodynamic wake width and length for the models studied in this research. It indicates a significant drag reduction. Two models using the JBT method are observed experimentally using Stereoscopic PIV. The wake area reductions are observed in the measured mean total velocity contour plots and in the mean Vx velocity profiles at 1.5 model lengths from the base of the models. Wind tunnel tests have documented that the smaller inlet area and passive jet slot result in a similar wake area reduction to that of the 4.7 times larger jet inlet area associated with the Jet2 model. Key differences that contribute to the behavior of the wake region for each model are documented to be the orientation of the passive jet, their velocity magnitudes and corresponding velocity profiles. The Jet1 model initiates the large coherent structures and flow entrainment earlier than the baseline model even though the jet momentum is small. The Jet2 generates paired vortices in the shear layer due to the high jet momentum and entrain main flow to the base region. These measurements are also confirmed in the numerical investigations using LES. The high Reynolds number of Re= 2.6×10^6 is computationally simulated to mimic the high Reynolds number flow expected on a tracker-trailer. LES indicates that the JBT passive flow control is more effective at reducing the base drag at the high Reynolds numbers, which are outside the experimental limitation of the wind tunnel used.

References

1. Hucho W. H.. Aerodynamik des Automobils. Wieweg+ Teubner, fifth edition, 2005.
2. Drollinger, R., “Heavy Duty Truck Aerodynamics,” SAE Technical Paper 870001, 1987, doi:10.4271/870001
3. Buresti, G. and Iungo, G. V. and Lombardi, G., Methods for The Drag Reduction of Bluff Bodies and Their Application to Heavy Road-Vehicles. 1st Interim Report Contract between CRF and DIA, DDIA 2007-6, Oct.2007.
4. Storms, B. L. and Satran, D. R. and Heineck, J. T. and Walker, M., A Summary of the Experimental Results for aGeneric Tractor-Trailer in the Ames Research Center 7-by 10-Foot and 12-Foot Wind Tunnels. NASA/ TM2006-213489, 2006.
5. Diamond, S., Ed, Heavy Vehicle Systems Optimization. 2004 Annual Progress Report, Feb, 2005.
6. Tanner, M., Reduction of Base Drag, Prog. Aerospace Sci., vol. 16, No. 4, pp. 369384, 1975.
7. Maull, D. J. and Hoole B. J.,, The effect of boat-tailing on the flow around a two-dimensional blunt-basedaerofoil at zero incidence, J. Royal Aero. Soc., vol. 71, pp. 854858, 1967.
8. McCallen, R., DOEs Effort to reduce truck aerodynamic drag through joint experiments and computations. Presentation at the DOE Heavy Vehicle Systems Optimization Merit Review and Peer Evaluation, Argonne National Laboratory, April 18-20, 2006.
9. Berman, P. W., Investigation into the effect of base bleed on the flow behind a two-dimensional model with a blunt trailing edge. AGARD CP-4, Part 2, pp. 485-507, 1966.
10. Zha, G.-C., Low Noise and Low Drag Automobile Mirrors Using Jet Flow Control, UMM-115, University of Miami Invention Disclosure, Sept. 7, 2012.
11. Zha, G.-C., Low Noise Low Drag Automobile Mirrors, Provisional Patent filed to USPTO,61/765,219, 02/15/2013, 2013.
12. Zha, G.-C., Low Drag Low Noise Automobile Mirrors Using Jet Flow Control, Patent Coorperation Treaty, PCT/ US2013/053191, filed to USPTO, 08/01/2013, 2013.
13. Zha, G.-C., Low Drag Low Noise Device Using Jet Flow Control, Utility Patent filed to USPTO on 02/14/2014, 14/180,460.
14. Wang, J., Bartow, W., Moreyra, A., Woyczynski, G. et al., “Low Drag Automotive Mirrors Using Passive Jet Flow Control,” SAE Int. J. Passeng. Cars - Mech. Syst. 7(2): 2014, doi:10.4271/2014-01-0584.
15. Engineering Laboratory Design, INC. “Model 406,” http://www.eldinc.com/pages/Model406/, 2009
16. Kirk, D., Experimental and Numerical Investigations of a High Performance Co-Flow Jet Airfoil, Masters Thesis, Mechanical Engineering Department, University of Miami, Coral Gables, 2009.
17. Litron Lasers, “Lasers for PIV Applications” http://www.litronlasers.com/pdf%20files/LitronPIVProducts0109_1.pdf
18. International Towing Tank Conference Recommended Procedures and Guidelines, Uncertainty Analysis Particle Imaging Velocimetry, Sept. 2008.
19. Anderson, J.D., “Fundamentals of Aerodynamics,” McGraw-Hill, Boston, ISBN 0-07-339810-1, 2001.
20. Wu, J.Z., Ma, H.Y., Zhou, M.D., Vorticity and Vortex Dynamics, Springer, 2006, Berlin.
21. Shen, Y.-Q. and Zha, G.-C. and Chen, X.-Y., High Order Conservative Differencing for Viscous Terms and the Application to Vortex-Induced Vibration Flows, Journal of Computational Physics, vol. 228(2), pp. 82838300, 2009.
22. Roe, P. “Approximate Riemann Solvers, Parameter Vectors, and Difference Schemes”, “Journal fo Computational Physics”, 1981.
23. Shen, Y.-Q. and Zha, G.-C. and Wang, B.-Y., “Improvement of Stability and Accuracy of Implicit WENO Schem,” AIAA Journal, Vol.47, No. 2, pp. 331-344, 2009.

$\boldsymbol{\rho}$ - Density

$\boldsymbol{\tau}$ - Surface Shear Stress

$\mathbf{C_d}$ - Drag Coefficient

Fx,Fy,Fz - Force components in the x,y,z directions

L - Distance of reference length

$\mathbf{p_\infty}$ - Free Stream Pressure

TKE - Turbulent Kinetic Energy

$\mathbf{u_\infty}$ - Free Stream Velocity

u - Flow Velocity

u′ - Fluctuating component of Velocity

U,V,W - velocity components in the x, y, z direction

$\mathbf{V_{Total}}$ - Planar Velocity including U and V components

The Engineering Meetings Board has approved this paper for publication. It has successfully completed SAE's peer review process under the supervision of the session organizer. This process requires a minimum of three (3) reviews by industry experts.

ISSN 0148-7191

http://papers.sae.org/2014-01-2448